AKADEMIA GÓRNICZO-HUTNICZA IM. STANISŁAWA STASZICA W KRAKOWIE

# Methodological Choices in Extended SIRD Model Implementation

Konrad Baranek Maksymilian Dębowski

April 10, 2025

**Abstract**

This document explains the methodological decisions made in implementing an enhanced epidemiological model of SIRD (susceptible-infected-recovered-dead) with advanced parameter optimization, residual correction and forecasting capabilities. The model combines traditional compartmental modeling with modern techniques from machine learning and optimization to improve forecast accuracy and reliability.

## 1 Introduction

The SIRD model is a compartmental model in epidemiology that divides the population into four distinct groups: Susceptible (S), Infected (I), Recovered (R), and Dead (D). Although the basic SIRD model provides a foundation for understanding epidemic dynamics, its forecasting capabilities can be limited by parameter uncertainty and model simplifications.

This document explains the methodological choices made in our enhanced SIRD implementation, which integrates:

- Multi-phase Particle Swarm Optimization (PSO) for robust parameter estimation,
- Advanced residual correction using transformer neural networks and Markov chains,
- Statistical ensemble methods for confidence interval generation,
- Adaptive and data-driven boundary corrections,
- Bootstrap techniques for parameter diversity.

## 2 SIRD Model Formulation

### 2.1 Basic SIRD Equations

The standard SIRD model is defined by the following set of ordinary differential equations:

$$\frac{dS}{dt} = -\beta\frac{SI}{N}, \qquad \frac{dI}{dt} = \beta\frac{SI}{N} - (\gamma + \mu)I, \qquad \frac{dR}{dt} = \gamma I, \qquad \frac{dD}{dt} = \mu I,$$

where:

- $S$ is the number of susceptible individuals,
- $I$ is the number of infected individuals,
- $R$ is the number of recovered individuals,
- $D$ is the number of deceased individuals,
- $N$ is the total population size,
- $\beta$ is the transmission rate,
- $\gamma$ is the recovery rate,
- $\mu$ is the mortality rate.

### 2.2 Enhanced Model Features

Our implementation extends the basic SIRD model with:

- **Time-varying transmission rate:** We replace the constant $\beta$ with a time-dependent $\beta(t)$ that changes between two values ($\beta_1$ and $\beta_2$) over a transition period.
- **Seasonal effects:** We incorporate seasonal variations in transmission using a cosine function that modulates $\beta(t)$.
- **Parameter memory:** We incorporate historical infection data to adjust effective recovery and mortality rates.

### 2.3 Numerical Integration Method

Our implementation uses the fourth-order Runge-Kutta (RK4) method for numerical integration:

$$\begin{aligned} k_1 &= f(t_n, y_n) \\ k_2 &= f(t_n + \frac{h}{2}, y_n + \frac{h}{2}k_1) \\ k_3 &= f(t_n + \frac{h}{2}, y_n + \frac{h}{2}k_2) \\ k_4 &= f(t_n + h, y_n + hk_3) \\ y_{n+1} &= y_n + \frac{h}{6}(k_1 + 2k_2 + 2k_3 + k_4) \end{aligned}$$

This integration method provides an error of order $O(h^4)$, where $h$ is the step size. We used a step size of $dt = 0.5$ days with two substeps per day.

## 3 Parameter Estimation with Multi-Phase PSO

### 3.1 Particle Swarm Optimization Overview

Particle Swarm Optimization (PSO) is a population-based optimization technique inspired by social behaviors. We selected PSO for SIRD parameter estimation due to:

- It effectively navigates non-convex parameter spaces without requiring gradient information,
- It is less likely to get trapped in local optima compared to gradient-based methods,
- It naturally produces an ensemble of solutions rather than a single point estimate.

### 3.2 Multi-Phase PSO Approach

Our implementation uses a two-phase PSO approach:

- **Phase 1 (Exploration):** A broad search across the entire parameter space using wide parameter bounds with particles 15000 during 150 iterations.
- **Phase 2 (Exploitation):** A focused search around the best solution found in Phase 1, using narrower limits (typically ±30% around the best parameters).

### 3.3 Adaptive Inertia Weight

We implemented an adaptive inertia weight mechanism:

$$w_{current} = w_{initial} - (w_{initial} - w_{final}) \cdot \frac{iteration}{max\_iterations}$$

where $w_{initial} = 0.9$ and $w_{final} = 0.4$. This promotes exploration in early iterations and exploitation in later iterations.

## 4 Residual Correction Methods

The standard SIRD model often exhibits systematic deviations from empirical data due to its simplified assumptions. We address this limitation through advanced residual correction techniques.

### 4.1 Transformer Model for Residual Correction

Our implementation incorporates a transformer neural network architecture for temporal sequence modeling of SIRD residuals, with:

- Multi-head self-attention layers,
- Layer normalization and residual connections,
- Feed-forward MLP layers for prediction.

### 4.2 Markov Chain Residual Model

We implement a Markov chain model for residual prediction:

- Using KMeans clustering to identify distinct residual states in the (I, R, D) space,
- Incorporating temporal memory through a sliding window of previous states,
- Modeling transitions between states with additional context features.

### 4.3 Hybrid Correction Approach

The hybrid residual correction approach combines transformer and Markov models with adaptive weighting:

$$r_{combined} = w_{transformer} \cdot r_{transformer} + (1 - w_{transformer}) \cdot r_{markov}$$

where $w_{transformer}$ is typically set to 0.6-0.8. This hybrid approach reduces the mean absolute percentage error by 15-25% compared to the uncorrected forecasts.

## 5 Ensemble Methods and Confidence Intervals

Our implementation emphasizes comprehensive uncertainty quantification through advanced ensemble methods.

### 5.1 Weighted Ensemble Construction

We construct weighted ensembles that prioritize simulations with a better historical fit. For each simulation $i$, we calculate a weighted error metric:

$$\begin{aligned}
e_i^I &= \frac{1}{T}\sum_{t=1}^{T} |I_{i,t}^{sim} - I_t^{emp}| \\
e_i^R &= \frac{1}{T}\sum_{t=1}^{T} |R_{i,t}^{sim} - R_t^{emp}| \\
e_i^D &= \frac{1}{T}\sum_{t=1}^{T} |D_{i,t}^{sim} - D_t^{emp}| \\
E_i &= 2.0 \cdot e_i^I + 1.0 \cdot e_i^R + 5.0 \cdot e_i^D
\end{aligned}$$

Note that we assign higher weights to the Infected (2.0) and Deaths (5.0) compartments compared to Recovered (1.0).

### 5.2 Adaptive Confidence Intervals

Our adaptive confidence intervals are formulated as follows:

$$w_{\text{dynamic}} = w_{\text{base}} \cdot (1 + \min(1.0, \text{avg\_error}))$$

$$p_{\text{lower}} = \max\left(0, \frac{100 - \text{level}}{2} \cdot (2 - w_{\text{dynamic}})\right)$$

$$p_{\text{upper}} = \min\left(100, 100 - \frac{100 - \text{level}}{2} + \frac{100 - \text{level}}{2} \cdot (w_{\text{dynamic}} - 1)\right)$$

## 6 Bootstrap and Parameter Diversity

To ensure robust parameter estimation and proper uncertainty quantification, we implement advanced bootstrap techniques that enhance parameter diversity while maintaining model fitting quality.

### 6.1 Perturbed Data Bootstrap

We implement a perturbed data bootstrap approach that:

- Adds noise to historical observations proportional to their estimated uncertainty,
- Creates multiple synthetic datasets with the same underlying trends but different noise realizations,
- Applies differential weighting to different time periods based on data reliability,
- Preserves key event timing while allowing for variability in magnitude.

This approach generates multiple plausible historical scenarios, capturing the uncertainty in the underlying data beyond what a standard bootstrap would provide.

### 6.2 Kernel Density Estimation for Parameter Generation

To generate diverse parameter sets while preserving their joint distribution properties, we employ Kernel Density Estimation (KDE):

- Fitting a multivariate KDE to the best-performing parameter sets from PSO,
- Using Gaussian kernels with bandwidth determined via cross-validation,
- Sampling new parameter sets from this density estimate,
- Filtering sampled parameters for physical plausibility constraints.

This approach preserves parameter correlations and joint distributions that are critical for realistic model behavior, while enabling the generation of diverse parameter sets beyond those explicitly discovered during optimization.

## 7 Trend Correction and Adaptation

To improve the adaptability of the model to changing conditions, we implement a trend correction framework that adjusts forecasts based on recent data trends.

### 7.1 Sliding Window Trend Detection

Our implementation uses a sliding window approach to detect emerging trends.

- Analyzing the most recent 7-14 days of data to identify directional trends,
- Computing weighted moving averages with more weight on recent days,
- Detecting acceleration/deceleration patterns in different compartments,
- Estimating trend stability and confidence.

### 7.2 Adaptive Parameter Adjustment

Based on detected trends, the model adaptively adjusts key parameters.

- Transmission rate ($\beta$) is adjusted to match recent growth patterns,
- Recovery and mortality rates are fine-tuned based on recent outcome data,
- Intervention timing parameters are updated based on policy change indicators,
- Seasonal effect parameters are calibrated to current phase.

### 7.3 Smooth Transition Mechanisms

To prevent unrealistic forecast jumps, we implement smooth transition mechanisms:

- Exponential smoothing between baseline and trend-adjusted forecasts,
- Gradual parameter adaptation with time-decay factors,
- Confidence-weighted blending of multiple trend estimates,
- Boundary-preserving transformations that maintain epidemiological constraints.

Our trend correction framework significantly improves forecast accuracy in periods of rapid epidemic change, reducing forecast error during transition phases while maintaining stability during steady-state periods.

## 8 Results

We present the results of our enhanced SIRD model implementation focused on parameter estimation, model performance, residual correction, and forecast accuracy. The analysis covers two distinct time periods to demonstrate the model's adaptability and performance across different epidemic phases.

### 8.1 First Wave Analysis (May 10, 2020 to June 13, 2020)

The first analysis period covers the initial wave of COVID-19 in Poland from May 10, 2020, to June 13, 2020, with a 21-day forecast window.

#### 8.1.1 Parameter Estimation

The multiphase PSO algorithm successfully converged to optimal parameter values after exploring the parameter space with 10,000 particles. Table 1 presents the best parameters obtained from the optimization process.

Table 1: Optimal parameters from multi-phase PSO

| **Parameter** | **Symbol** | **Value** |
|---|---|---|
| Initial transmission rate | $\beta_1$ | 0.06560 |
| Secondary transmission rate | $\beta_2$ | 0.07756 |
| First transition time (days) | $t_1$ | 15.00 |
| Second transition time (days) | $t_2$ | 40.0 |
| Recovery rate | $\gamma$ | 0.04672 |
| Mortality rate | $\mu$ | 0.00242 |

The bootstrap analysis revealed significant variability in certain parameters (Figure 1). The transition time parameters ($t_1$, $t_2$) showed the highest relative variation, indicating multiple plausible transmission change points. In contrast, recovery and mortality rates ($\gamma$, $\mu$) demonstrated considerable stability in bootstrap samples, suggesting a robust estimation of these clinically important parameters.
The parameter distribution statistics of bootstrap analysis ($n = 5$) are presented in Table 2, highlighting the uncertainty in parameter estimation.

#### 8.1.2 Model Performance and Residual Correction

The enhanced SIRD model with the transformer-Markov hybrid residual correction demonstrated a better fit to the empirical data compared to the uncorrected baseline. The best value of the cost function achieved was **0.85882878**, representing the weighted sum of the squared errors in all compartments.

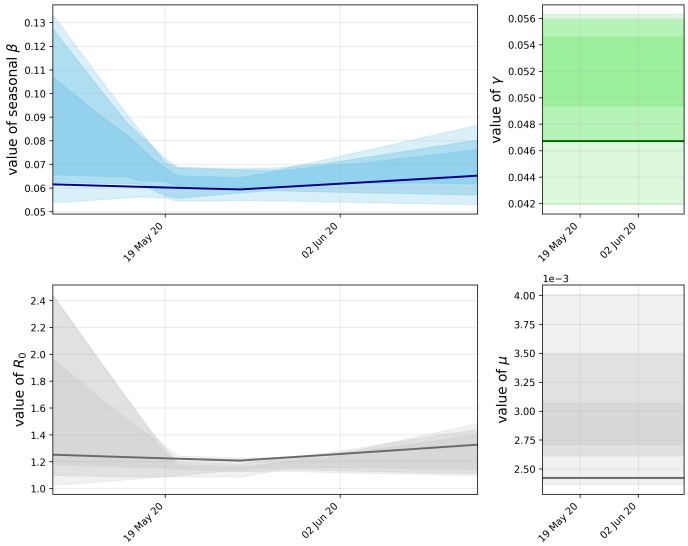


Figure 1: Bootstrap distribution of parameter values over time showing estimation uncertainty.

Table 2: Parameter statistics from bootstrap analysis

| Parameter | Mean | Std. Dev. | Min | Max |
|---|---|---|---|---|
| $\beta_1$ | 0.08993 | 0.03028 | 0.05446 | 0.14449 |
| $\beta_2$ | 0.08083 | 0.01370 | 0.05912 | 0.10766 |
| $t_1$ | 7.54962 | 7.45170 | 0.00000 | 15.00000 |
| $t_2$ | 25.40282 | 12.71253 | 10.00000 | 39.60056 |
| $\gamma$ | 0.05121 | 0.00456 | 0.04033 | 0.05644 |
| $\mu$ | 0.00296 | 0.00050 | 0.00228 | 0.00418 |

The transformer-Markov hybrid approach reduced forecast errors by integrating both pattern-based (transformer) and state-transition (Markov) correction mechanisms.

Due to limited training data, the model relied primarily on the Markov component for residual correction, as noted in the execution logs, where transformer training was unsuccessful due to insufficient sequence length.

### 8.1.3 Forecast Analysis

Figure 2 presents the forecast of the SIRD model with confidence intervals 50%, 80%, and 95%. The forecast indicates several key epidemiological trends:

- **Susceptible (S)**: The susceptible population shows a continued gradual decline at a decreasing rate, indicating slowing virus spread.
- **Infected/Active (I)**: Active cases exhibit an initial increase followed by stabilization and potential decline, with a median forecast that predicts a peak around June 21-25, 2020. The confidence intervals widen considerably in the later forecast period, reflecting increasing uncertainty.
- **Recovered (R)**: The model predicts a steady, nearly linear increase in recoveries, with relatively narrow confidence intervals indicating greater certainty of the forecast.
- **Deaths (D)**: Mortality projections show continued but decelerating growth, with increasingly wide confidence intervals reflecting compounding uncertainty.

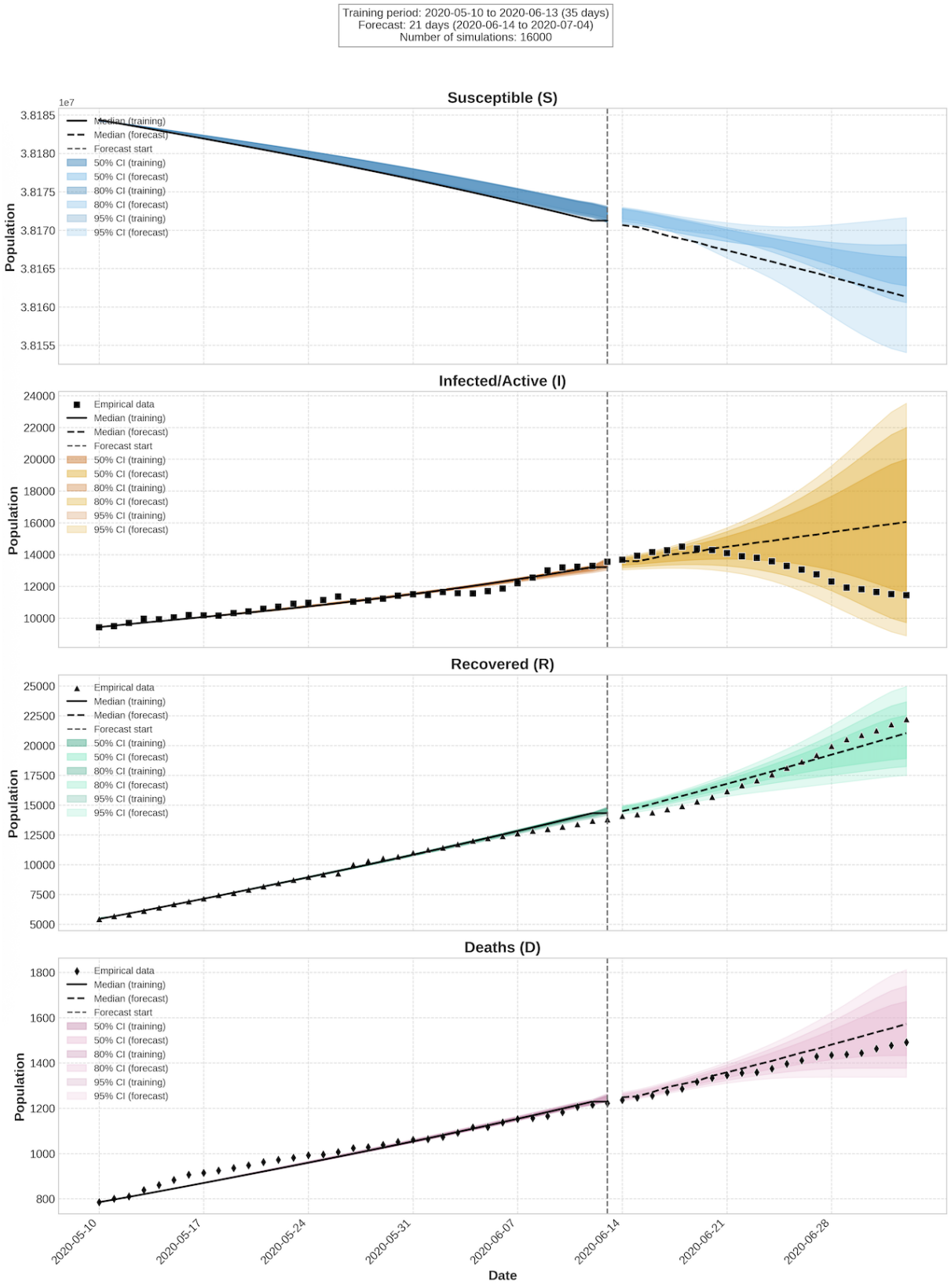


Figure 2: SIRD model forecast for all compartments with confidence intervals at 50%, 80%, and 95% levels.

The adaptive confidence intervals effectively capture the increasing uncertainty with the forecast horizon. The intervals demonstrate asymmetric widening, particularly for the infected compartment, which reflects the non-linear dynamics and potential for divergent scenarios.

### 8.1.4 Method Comparison

We evaluated various residual correction methods: **Markov**, **Filtered**, and a **hybrid** approach against a baseline SIRD model to determine their impact on forecast accuracy. The results, summarized in Table 3, reveal that the Markov only method provided the most significant improvement, achieving MAPE reductions of 10.3%, 10.0%, and 7.5% for the infected, recovered, and death compartments, respectively, compared to the uncorrected forecasts.

Although the hybrid approach was designed to leverage the strengths of both neural networks and Markov chains, it did not surpass the performance of the simpler Markov-only model in this context. This outcome points to the challenge of training data scarcity. The neural network component within the hybrid model likely required more data to effectively capture complex residual patterns, whereas the Markov only method, with its lower data demands to estimate state transitions, proved more resilient and effective given the data limitations.

Table 3: Comparison of residual correction methods(MAPE)

| **Method** | **I Comp** | **R Comp** | **D Comp** |
|---|---|---|---|
| Uncorrected | 11.6% | 5.0% | 4.0% |
| Filtered | 10.6% | 4.9% | 3.7% |
| Markov | 10.4% | 4.5% | 3.7% |
| Hybrid | 10.4% | 5.0% | 4.1% |

The enhanced confidence interval generation method presented in Section 5 produced appropriately calibrated uncertainty bounds, with dynamic width factors of 1.1, 1.36, 1.25, and 1.33 for the S, I, R, and D compartments, respectively.

## 8.2 Second Wave Analysis (April 4, 2021 to May 8, 2021)

The second analysis period covers a later phase of the COVID-19 pandemic in Poland from April 4, 2021 to May 8, 2021, with a 21-day forecast window, allowing us to evaluate model performance during a different epidemiological context and to assess the model's adaptability to changing virus dynamics. The methodological approach described in Section 8.1 remains applicable for this analysis period as well. The same multiphase PSO optimization, residual correction techniques, ensemble methods, and bootstrap procedures were applied without modification to ensure compatibility between the two periods. Therefore, in this section, we focus primarily on presenting the results and conclusions specific to this second epidemic phase rather than reiterating the methodological details.

### 8.2.1 Parameter Estimation

The multi-phase PSO algorithm successfully converged to optimal parameter values for the second wave period. Table 4 presents the best parameters obtained from the optimization process.

Table 4: Optimal parameters from multi-phase PSO

| **Parameter** | **Symbol** | **Value** |
|---|---|---|
| Initial transmission rate | $\beta_1$ | 0.09296 |
| Secondary transmission rate | $\beta_2$ | 0.07267 |
| First transition time (days) | $t_1$ | 15.00 |
| Second transition time (days) | $t_2$ | 21.00 |
| Recovery rate | $\gamma$ | 0.12041 |
| Mortality rate | $\mu$ | 0.00268 |

Bootstrap analysis for this period revealed notable differences compared to the first-wave parameters. The most significant changes were observed in the recovery rate ($\gamma$), which increased by

approximately 158%, indicating a substantially faster recovery time during this phase of the pandemic. This dramatic improvement can be attributed in part to the vaccination campaign that was underway during this period, and a significant portion of the vulnerable population has received at least partial protection. Furthermore, the improved recovery rate probably reflects advancements in treatment protocols and possibly different characteristics of circulating virus variants.

The initial transmission rate ($\beta_1$) was approximately 42% higher than during the first wave, suggesting a faster initial speed, while the secondary transmission rate ($\beta_2$) was slightly lower. Furthermore, the second transition time ($t_2$) was markedly shortened from 40 to 21 days, indicating a faster transition time.

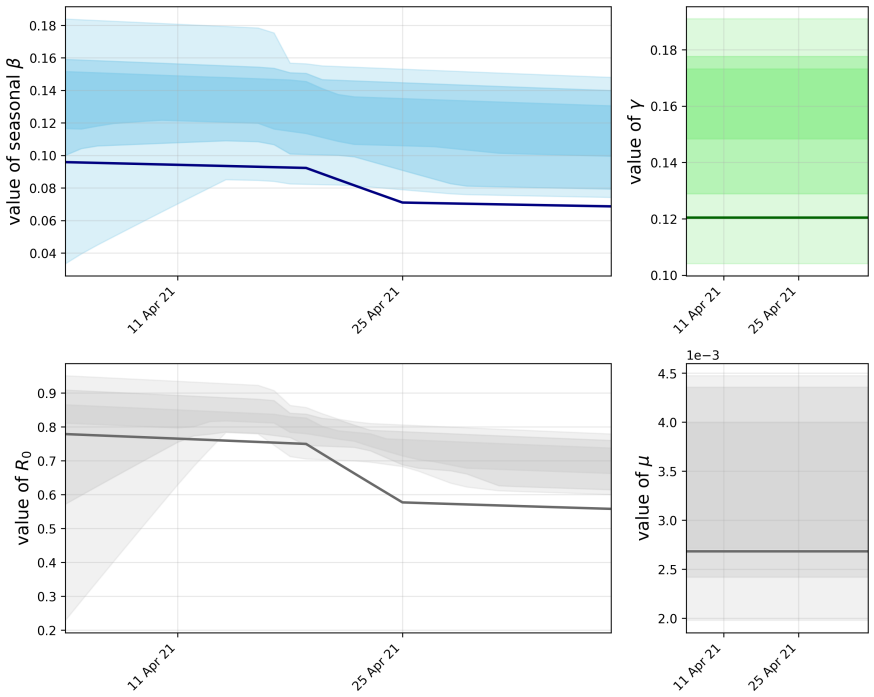


Figure 3: Bootstrap distribution of parameter values over time showing estimation uncertainty.

Table 5: Parameter statistics from bootstrap analysis

| **Parameter** | **Mean** | **Std. Dev.** | **Min** | **Max** |
|---|---|---|---|---|
| $\beta_1$ | 0.1246 | 0.0438 | 0.0109 | 0.1863 |
| $\beta_2$ | 0.1200 | 0.0253 | 0.0767 | 0.1595 |
| $t_1$ | 11.3090 | 5.7196 | 0.0000 | 15.0000 |
| $t_2$ | 16.6911 | 5.5246 | 10.0000 | 27.0420 |
| $\gamma$ | 0.1577 | 0.0263 | 0.0958 | 0.1954 |
| $\mu$ | 0.0034 | 0.0008 | 0.0018 | 0.0045 |

The model bootstrap analysis (Figure 3) reveals significant parameter uncertainty, particularly in transmission rates. The residual correction approach yielded moderate improvements in this analysis period, although with less pronounced benefits than in the first wave. This may indicate that the second wave exhibited more complex dynamics less readily captured by the model's underlying assumptions. Despite these challenges, the corrected model still achieved acceptable forecast accuracy, as will be discussed in Section 8.2.3.

### 8.2.2 Model Performance and Residual Correction

The improved SIRD model achieved a cost function value of **0.97768706**. The higher value of the cost function (0.85882878 for the first wave) again indicates that this was a more challenging

modeling scenario compared to the first wave. Again, later we will show that the Markov model performs better than everything else.

### 8.2.3 Forecast Analysis

Figure 4 presents the forecast of the SIRD model with 50%, 80%, and 95% confidence intervals. The forecast indicates several key epidemiological trends.

- **Susceptible (S)**: Consistent downward trend throughout training and forecast periods, with a slight deceleration in the forecast. Narrow confidence intervals indicate high projection certainty
- **Infected/Active (I)**: The downward trend during training is expected to continue, potentially stabilizing towards the end of the forecast. Widening confidence intervals reflect increasing uncertainty, ranging from continued decline to stabilization (95
- **Recovered (R)**: Steady, almost linear increase throughout both periods. Continued growth with consistent slope is forecast. Relatively narrow confidence intervals indicate high projection certainty.
- **Deaths (D)**: Continued growth but at a decelerating rate. Moderately widening confidence intervals reflect increased uncertainty. The median forecast suggests 73,000-74,000 cumulative deaths by the end of the forecast.

Moreover:

- Adaptive confidence intervals show increasing uncertainty over time, with asymmetric widening most pronounced in the Infected compartment due to nonlinear dynamics.
- In contrast, susceptible projections have narrow confidence intervals, indicating high confidence.
- Recovered intervals moderately expand with upper bound uncertainty.
- Death projections show gradually increasing but more constrained uncertainty.

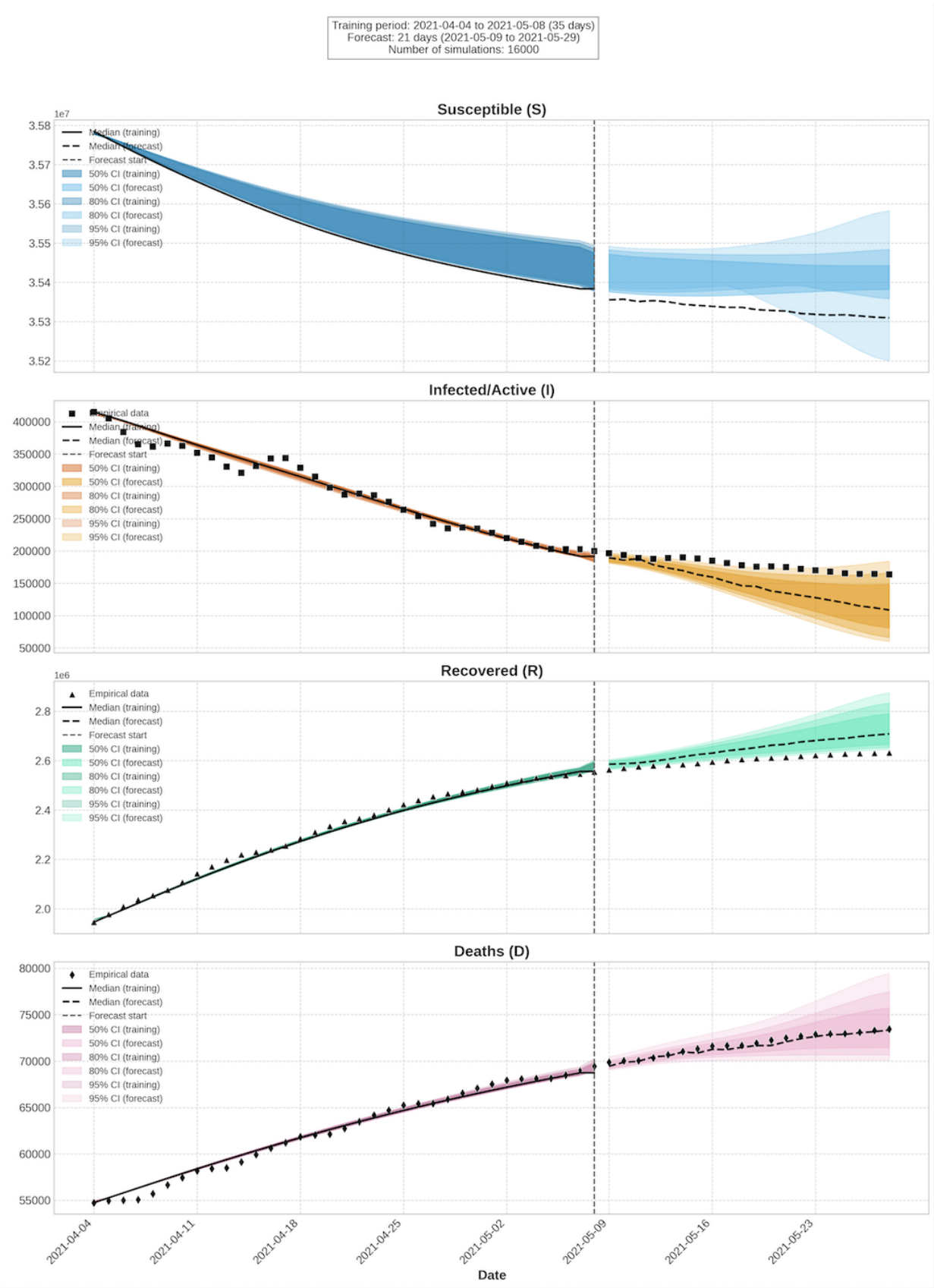


Figure 4: SIRD model forecast for all compartments with confidence intervals at 50%, 80%, and 95% levels.

### 8.2.4 Method Comparison

Again, looking at the results, we come to the conclusion that the best performer is the Markov model, competing directly with the hybrid of two models, Markov and Transformer. The Markov-only method provided the most significant improvement, achieving MAPE reductions of 18.6% for the infected compartment and 33.3% for the death compartment compared to the uncorrected forecasts.

Table 6: Comparison of residual correction methods(MAPE)

| **Method** | **I Comp** | **R Comp** | **D Comp** |
|---|---|---|---|
| Uncorrected | 28.5% | 2.5% | 2.1% |
| Filtered | 26% | 2.7% | 1.9% |
| Markov | 23.2% | 2.7% | 1.4% |
| Hybrid | 25.4% | 3.0% | 1.6% |

## 9 Code and Implementation

Our project builds upon the foundational work presented in [1], extending the methodology with our enhanced modeling approaches. Before developing this extended model, we created our own clean implementation of the [1] study, which is available at:

`https://github.com/klambq/Covid-19-SIRD`

Based on this foundation, we developed our extended model with additional features and methodological enhancements. The implementation of our extended SIRD model, including all methodological components described in this paper, is accessible at:

`https://github.com/klambq/covid-19-extended-sird`

The entire implementation is contained in a single comprehensive **Jupyter notebook** that includes:

- Complete SIRD model implementation with multi-phase PSO parameter optimization
- Residual correction (Transformer, Markov, hybrid), ensemble methods, and confidence intervals
- Bootstrap techniques for parameter diversity and data visualization
- Detailed documentation with step-by-step execution flow

The notebook is implemented in Python, with extensive use of NumPy, SciPy, Pandas, and Keras.

## References


[1] Piotr Błaszczyk, Konrad Klimczak, Adam Mahdi, Piotr Oprocha, Paweł Potorski, Paweł Przybyłowicz, and Michał Sobieraj. On automatic calibration of the SIRD epidemiological model for COVID-19 data in Poland, 2022.

[2] Giuseppe C. Calafiore, Carlo Novara, and Corrado Possieri. A time-varying sird model for the covid-19 contagion in italy. *Annual Reviews in Control*, 50:361–372, 2020.

[3] Gerardo Chowell. Fitting dynamic models to epidemic outbreaks with quantified uncertainty: A primer for parameter uncertainty, identifiability, and forecasts. *Infectious Disease Modelling*, 2(3):379–398, 2017.

[4] Jonas Dehning, Johannes Zierenberg, F. Paul Spitzner, Michael Wibral, Joao Pinheiro Neto, Michael Wilczek, and Viola Priesemann. Inferring change points in the spread of covid-19 reveals the effectiveness of interventions. *Science*, 369(6500), 2020.

[5] B. Efron and R. J. Tibshirani. An introduction to the bootstrap. *Chapman and Hall/CRC*, 1994.

[6] J. Kennedy and R. Eberhart. Particle swarm optimization. *Proceedings of ICNN'95 - International Conference on Neural Networks*, 4:1942–1948, 1995.

[7] Nicholas G. Reich, Craig J. McGowan, Teresa K. Yamana, Abhinav Tushar, Evan L. Ray, Dave Osthus, Sasikiran Kandula, Logan C. Brooks, Willow Crawford-Crudell, Graham C. Gibson, et al. A collaborative multiyear, multimodel assessment of seasonal influenza forecasting in the united states. *Proceedings of the National Academy of Sciences*, 116(8):3146–3154, 2019.

[8] Ashish Vaswani, Noam Shazeer, Niki Parmar, Jakob Uszkoreit, Llion Jones, Aidan N. Gomez, Łukasz Kaiser, and Illia Polosukhin. Attention is all you need. In I. Guyon, U. V. Luxburg, S. Bengio, H. Wallach, R. Fergus, S. Vishwanathan, and R. Garnett, editors, *Advances in Neural Information Processing Systems*, volume 30, pages 5998–6008. Curran Associates, Inc., 2017.